Precursor determined lateral size control of monolayer MoS_2 nanosheets from a series of alkylammonium thiomolybdates: A reversal of trend between growth media

Jack R. Brent[†a], Paul D. McNaughter[†b] and Paul O'Brien[a,b]*

[a]School of Materials, University of Manchester, Oxford Road, Manchester, UK M13 9PL

[b]School of Chemistry, University of Manchester, Oxford Road, Manchester, UK M13 9PL

† *Authors contributed equally*

Supporting information

Experimental information

Precursor Synthesis

Tetrabutyl tetrahexylammonium bromide (≥98.0 %, Sigma), tetrahexylammonium bromide (99 %, Sigma), tetraoctylammonium bromide (98 %, Sigma) ammonium tertathiomolybdate $[NH_4]_2[MoS_4]$ (99.95 %, Sigma), dichloromethane (≥99.8 % purity, amylene stabilized, Sigma), polystyrene (average Mw ~280,000, Sigma) NaOH (97 %, Fisher) and *N*-methyl-2-pyrrolidone (>99 %, Alfa Aesar). All reagents and solvents were used without further purification.

$[Bu_4N]_2[MoS_4]$ and $[Hex_4N]_2[MoS_4]$ were synthesized according to the method reported by Bensch et al (Z. Naturforsch. 2007, 62b, 209-214). $[R_4N]Br$ (20 mmol) and NaOH (20 mmol) were dissolved in 40 ml deionized (DI) water. $[NH_4]_2[MoS_4]$ (10 mmol) was dissolved in 40 ml DI water and the two solutions mixed dropwise under stirring to form a red-brown gel. The solution was stirred for 1 h and filtered, dried and recrystallized in hot acetonitrile. $[Bu_4N]_2[MoS_4]$ and $[Hex_4N]_2[MoS_4]$ were obtained as dry red powders.

$[Oct_4N]_2[MoS_4]$ was synthesized using the same method as $[Bu_4N]_2[MoS_4]$ and $[Hex_4N]_2[MoS_4]$ except that 30 ml of methanol was added to the 80 ml of water to allow mixing of the precursors. $[Oct_4N]_2[MoS_4]$ was obtained as a viscous red/brown oil and was dried *in vacuo* at 40 °C overnight.

Characterisation of Precursors

Tetrabutylammonium tetrathiomolybdate, $[Bu_4N]_2[MoS_4]$. Positive electrospray mass spectrometry shows a molecular ion peak at m/z 710.0, and larger clusters $[(Bu_4N)_3MoS_4]^+$ at m/z 952. Negative electrospray mass spectrometry shows molecular ion peak at m/z 709.5 as well as its dimer centered at m/z 1410.8 and $[(Bu_4N)_3(MoS_4)_2]^-$ at m/z 1176.7. Lower weight fragments are found at m/z 466.1$[(Bu_4N)MoS_4]^-$, m/z 282 $[(C_4H_9)MoS_4]^-$ and m/z 225.7 $[MoS_4]^-$.We assign the signals at m/z 466.1 and m/z 652.9 to $[(Bu_4N)MoS_4]^-$ and $[(Bu_3N)(Bu_4N)MoS_4]^-$ respectively. ^1H NMR (400 MHz, $CDCl_3$) δ 3.50 – 3.29 (m, 8H), 1.76 – 1.58 (m, 8H), 1.57 – 1.38 (m, 8H), 0.99 (t, *J*

= 7.3 Hz, 12H). Microanalysis was as follows: C 52.93% (expected 54.2%) H 10.66% (expected 10.23%) N 3.88% (expected 3.95%) S 18.22% (expected 18.09%). m.p. 167-169 °C

Tetrahexylammonium tetrathiomolybdate, $[Hex_4N]_2[MoS_4]$, Positive electrospray mass spectrometry shows protonated molecular ion peak at m/z 935.8 and clusters $[(Hex_4N)_3MoS_4]^+$ at m/z 1289.3 and $[(C_6H_{13})_2(C_6H_{13})NMoS_4]^+$ at m/z 743.8. Fragments $(C_6H_{13})_4N$ and $[MoS_4]^-$ are observed at m/z 354.8 and m/z 226 respectively. ^1H NMR (400 MHz, $CDCl_3$) δ 3.44 – 3.17 (m, 8H), 1.74 – 1.52 (m, 8H), 1.48 – 1.22 (m, 24H), 0.89 (t, *J* = 7.0 Hz, 12H). Microanalysis was as follows: C 59.91% (expected 61.75%) H 11.20% (expected 11.23%) N 2.94% (expected 3.00%) S 13.89% (expected 13.74%) m.p. 137 °C

Tetraoctylammonium tetrathiomolybdate, $[Oct_4N]_2[MoS_4]$. Negative ion electrospray shows a small expected molecular ion signal at m/z 1156.4 and fragments $[(C_8H_{17})_4N)MoS_4]^-$ at m/z 692.4 and $[MoS_4]^-$ at m/z 225.7. Positive electrospray shows $[(C_8H_{17})_4N)_3MoS_4]^+$ at m/z 1624 and $(C_8H_{17})_4N^+$ at m/z 467.0. $[MoS_3]^-$ at m/z 189.8 and $[(C_8H_{17})_4N]_2S^+$ at 968.2 are found in the negative and positive spectra respectively. ^1H NMR (400 MHz, $CDCl_3$) δ 3.38 – 3.11 (m, 8H), 1.71 – 1.50 (m, 8H), 1.48 – 1.23 (m, 40H), 0.88 (t, *J* = 6.9 Hz, 12H). Microanalysis was as follows: C 65.12% (expected 66.38%) H 12.06% (expected 11.84%) N 2.45% (expected 2.42%) S 10.06% (expected 11.08%).

TEM sample preparation

Polymer-MoS_2 films were immersed in a small amount of dichloromethane (DCM) in order dissolve the films. The dispersion of MoS_2 sheets and polystyrene had limited colloidal stability in DCM causing flocculation. The dispersions were rapidly drop casted on to TEM grids. Polymer-free films from melt reactions were placed in a small amount of NMP and ultrasonicated to liberate nanosheets.

Instrumentation

^1H NMR was carried out on a Bruker AVANCE III 400 MHz spectrometer. Electrospray mass spectrometry was carried out on Waters SQD2 Single Quadrupole Mass Spectrometer by the UoM School of Chemistry (SoC) Mass Spectrometry Service. Microanalysis and TGA was carried out by the UoM SoC Micro Analytical Laboratory.

Spin coating was carried out on an Ossila spin coater. Raman spectra were collected using a Renishaw 1000- Micro-Raman System equipped with a 514 nm laser operating at 1 mW. The system was calibrated against an SiO2 standard. SEM and EDX maps were obtained on a Phillips XL 30 FEG scanning electron microscope with DX4 detector. TEM investigations were carried out using a Tecnai T20 with a LaB_6 source and an Oxford XMax 80 TLE EDX detector. UV-visible spectroscopy was carried out on a Shimadzu UV1800 UV spectrophotometer with a 1 cm path length.

Supporting Figures

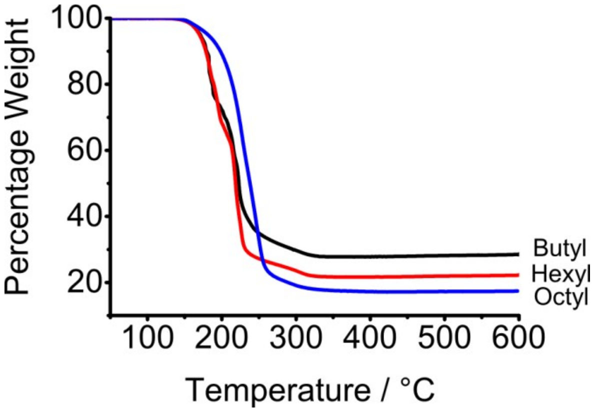

SI Figure 1: TGA profiles for $[R_4N]_2[MoS_4]$ with alkyl chain length in the annotation.

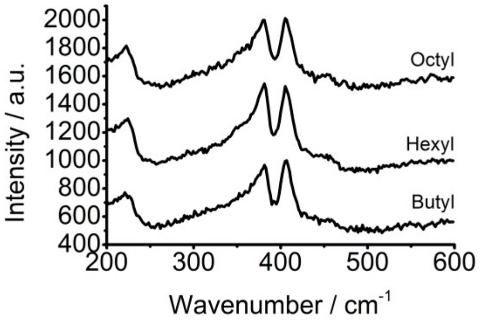

SI Figure 2: Raman spectra for films produce from melt reaction of $[R_4N]_2[MoS_4]$ with alkyl chain length in the annotation.

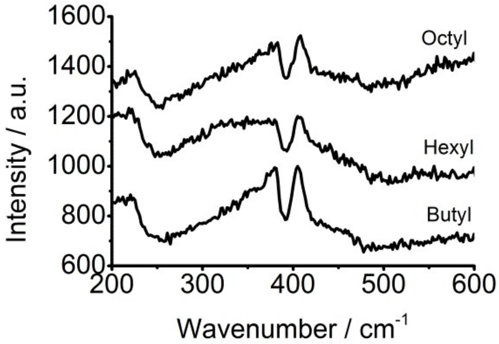

SI Figure 3: Raman spectra for films produce from *in situ* reaction of $[R_4N]_2[MoS_4]$ in polystyrene with alkyl chain length in the annotation.

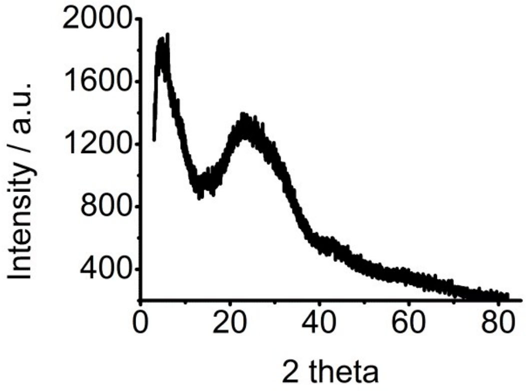

SI Figure 4: XRD diffraction pattern collected for the film produced from the melt reaction of $[Bu_4N]_2[MoS_4]$.

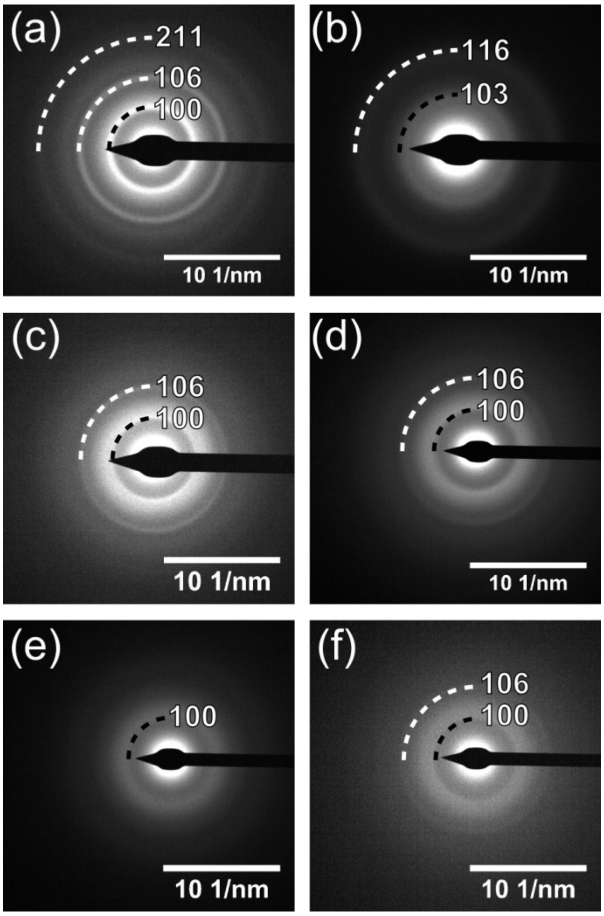

SI Figure 5: SAED patterns of the MoS_2 nanosheets produced with (a) melt using butyl precursor, (b) in polymer using butyl precursor, (c) melt using hexyl precursor, (d) in polymer using hexyl precursor, (e) melt using octyl precursor and (f) in polymer using octyl precursor. Patterns are matched against ICCD pattern # 00-024-0513.

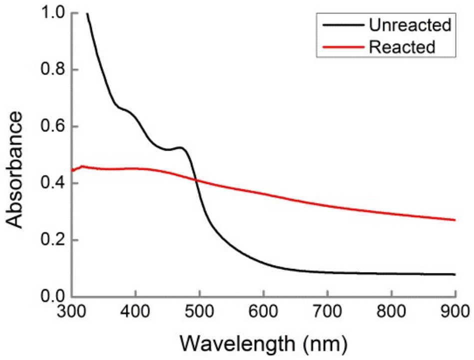

SI Figure 6: UV-vis spectra of the unreacted film of molecular precursors (black) and the reacted film (red).

SI Table 1: ICP-AES results and subsequent yield for Mo when $[Oct_4N]_2[MoS_4]$ was decomposed in a melt reaction.

	Value	Standard deviation
Mo content after heating (mol/ml)	4.89×10^{-3}	5.72×10^{-5}
Mo content before heating (mol/ml)	5.08×10^{-3}	3.48×10^{-5}
Mo after/Mo before	0.96	7.72×10^{-5}
Percentage Mo	96.24	7.72×10^{-3}

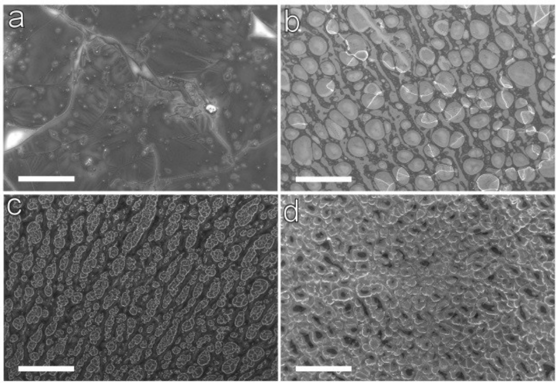

SI Figure 7: Representative SEM micrographs of spin-coated films prior to reaction of (a) $[Bu_4N]_2[MoS_4]$ (scale bar is 100 µm) and in polymer (b) $[Bu_4N]_2[MoS_4]$, (c) $[Hex_4N]_2[MoS_4]$ and (d) $[Oct_4N]_2[MoS_4]$ (scale bar is 500 µm).

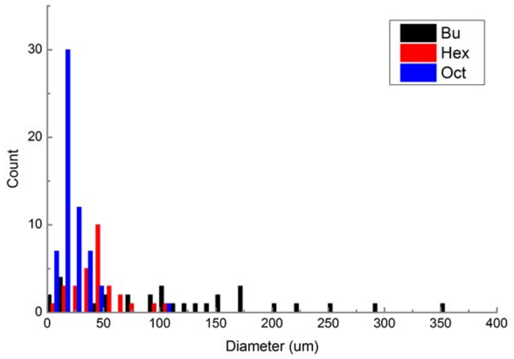

SI Figure 8: Combined domain size histograms for reacted films.

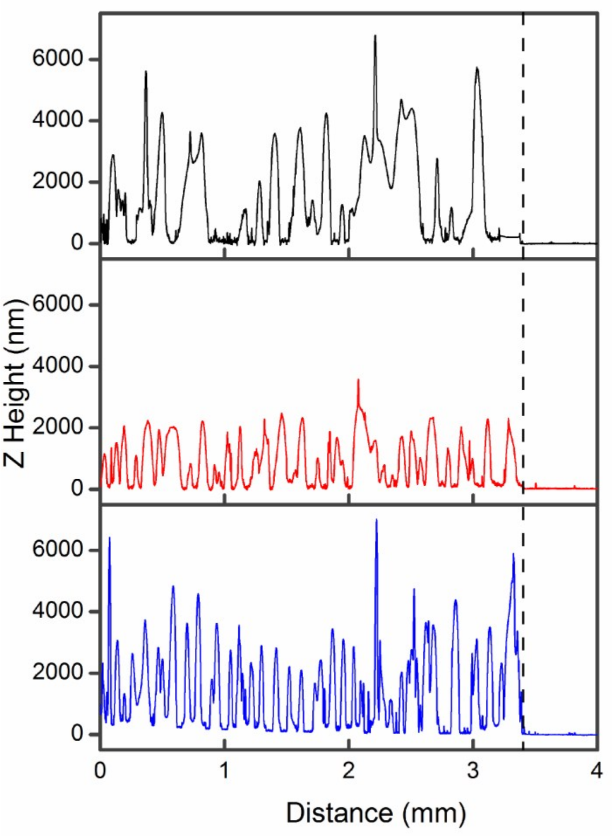

SI Figure 9: 1 dimensional surface profile measurements of MoS_2-polymer films made from using precursors (top) $[Bu_4N]_2[MoS_4]$, (middle) $[Hex_4N]_2[MoS_4]$ and (bottom) $[Oct_4N]_2[MoS_4]$. The black hashed line represents the point the film was removed to expose the glass substrate to allow film thickness to be determined.

SI Table 2: Average peak and trough heights relative to the substrate

Length of alkyl chain	Mean film thickness in trough / nm	Mean peak height / nm	Trough thickness as a percentage of peak height, %

Butyl	215	3203	6.7
Hexyl	111	1720	6.5
Octyl	56	3311	1.7

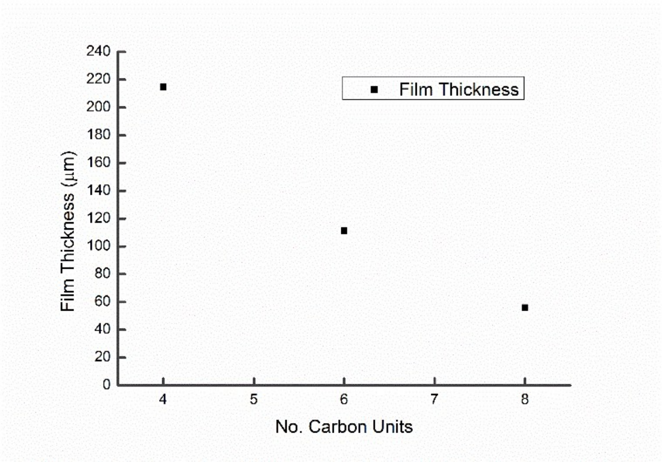

SI Figure 10: Thickness of the film within the elliptical domains when using $[R_4N]_2[MoS_4]$ where R = to butyl (4 carbons), hexyl (6 carbons) and octyl (8 carbons).

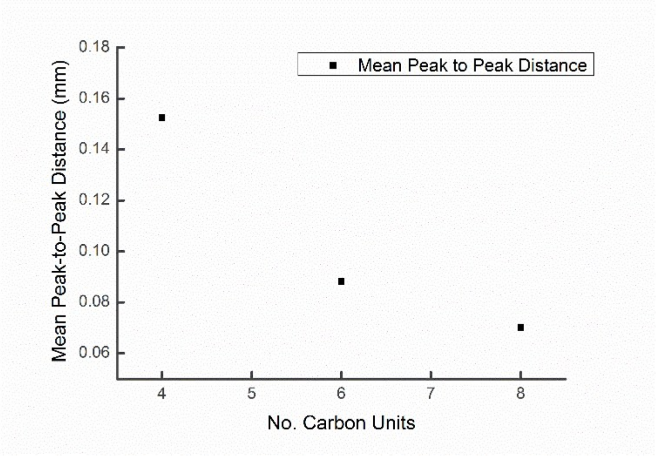

SI Figure 11: Width of elliptical structure, *i.e.* peak to peak distance, when using $[R_4N]_2[MoS_4]$ where R = to butyl (4 carbons), hexyl (6 carbons) and octyl (8 carbons).

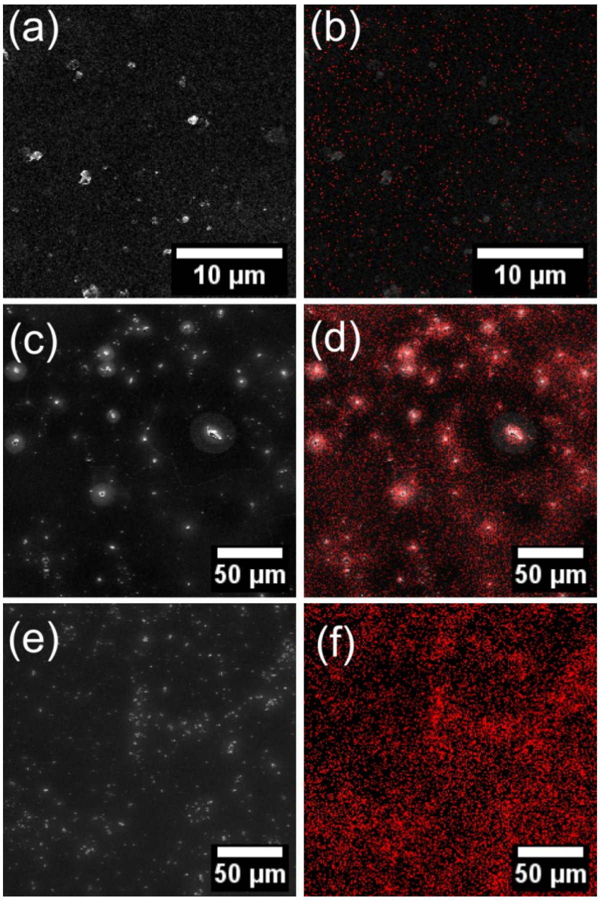

SI Figure 12: SEM micrographs and the corresponding Mo EDX spectroscopy maps for the films produced from the melt reactions of with (a & b) butyl precursor, (c & d) hexyl precursor and (e & f) octyl precursor.

Justification for making size measurements of rectangular sheets along their edge

We wish to find the relationship between edge lengths and observed length (L_{obs})

We may assume:

1) The particles in the system are randomly orientated
2) The sample is monodisperse.
3) Sheets may lie with their long axis L at any angle from the viewing plane between 0 and 90 degrees.

Definitions

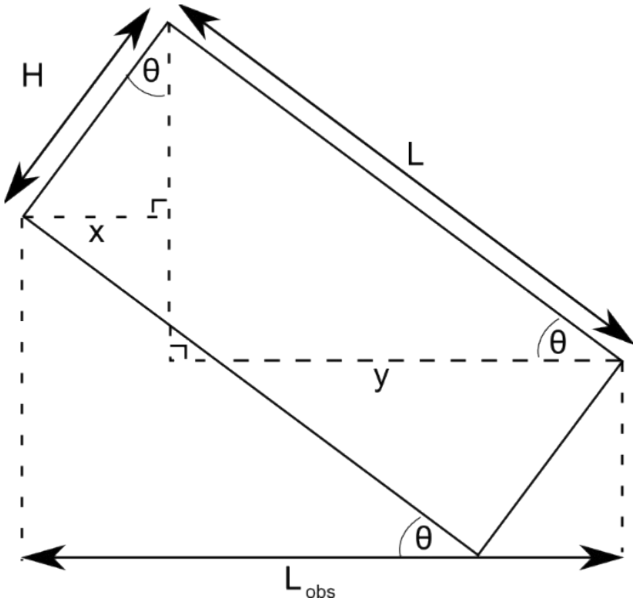

Extreme case 1: L = H (a square)

$L_{obs} = x + y$

$x = H \sin\theta$

$y = L \cos\theta$

$L_{obs} = H \sin\theta + L \cos\theta$

In this extreme case L = H

$L_{obs} = L \sin\theta + L \cos\theta$

$L_{obs} = L (\cos\theta + \sin\theta)$

$L_{obs} \approx 1.27\ L$

This makes sense as viewing a tilted square (H=L) from the side would result in an overestimate of the edge length.

Extreme case 2: L >> H, *i.e.* H= 0

$L_{obs} = H \sin\theta + L \cos\theta$

As H = 0

$L_{obs} = L \cos\theta$

$L_{obs} \approx 0.63\ L$

This also makes sense as viewing a very long and thin sheet would result in an underestimate of the length of the long axis.

Therefore, in the extreme cases $1.27\ L \geq L_{obs} \geq 0.63\ L$.